Analysis of superelevation and debris flow velocities at Illgraben, Switzerland

Amanda Åberg[1,2*], *Jordan* Aaron[2,1], *Tjalling* de Haas[3], *Brian* McArdell[1], *Jacob* Hirschberg[2,1]

[1]Swiss Federal Institute for Forest, Snow and Landscape Research WSL, CH8903 Birmensdorf, Switzerland
[2]Department of Earth Sciences, ETH Zürich, 8092 Zürich, Switzerland
[3]Department of Physical Geography, Utrecht University, 3584 CS Utrecht, the Netherlands

Abstract. The forced vortex equation, based on the cross-stream inclination of a flow surface as it passes through a bend, is a common approach to estimating debris flow velocities. Here, we present the preliminary results of a study of superelevation and the correction factor *k*, used to adapt the forced vortex equation to debris flows, based on data from the Illgraben torrent in Switzerland. The definition of the radius of curvature, a factor in the calculation of superelevation velocities, is not found to exercise a large influence on the calculated velocities when using high resolution aerial images, with the choice of cross-section location and *k*-factor exercising a more significant influence. The *k*-factors found here fall within the range previously reported in the literature, ranging from approximately 1 to 7, and a previously suggested non-linear relationship with Froude numbers is evident in the dataset. Following the debris flow season of 2022, the study will be continued with additional debris flow events and the investigative methods will be extended to include high-resolution LiDAR sensors installed along the Illgraben torrent.

1 Introduction

Hazard evaluations of debris flows are critically dependent on good estimates of debris flow velocity and discharge [1]. One commonly used method for post-hoc estimation of debris flow velocity is the superelevation approach, which is based on the cross-stream inclination of the flow surface as it experiences centripetal acceleration passing through a bend [2, 3]. Though initially used for pure water flows, the forced vortex equation has been adapted to non-Newtonian fluids such as debris flows by incorporating a correction factor *k* [4, 5]:

$$v_{df} = \left(\frac{R_c g^*}{Bk}\Delta h\right)^{0.5} \quad (1)$$

where g^* represents the bed-normal component of acceleration due to gravity, R_c the radius of curvature, Δh the difference in elevation of the flow surface between the inner and outer bend, and B the width of the flow. Note that eq. 1 is valid for rectangular cross-sections. The correction factor *k* has been suggested to be connected to the viscosity and vertical sorting of a debris flow [4, 6]. Literature values of *k* are typically between 1 to 5 [4, 6] but may be as high as 10 [7]. Further, *k*-values have been found to depend on the Froude number, converging to 1 for supercritical flow conditions and increasing exponentially for subcritical flow conditions [5, 8]. This was found both for experiments as well as *k*-factors derived from events at the Illgraben torrent. In addition to the uncertainties related to *k*, the definition of the radius of curvature for natural bends has been contentious because it is generally based on a subjective assessment and influenced by the scale of the media used [9].

Though the superelevation method is commonly used for post-hoc assessment of debris flow velocity, evaluation of the accuracy of the results is often difficult due to the lack of independent velocity reference data. In this study, we use high-resolution orthophotos and digital elevation models (DEM's), as well as independent front velocity estimates from the 2019-2021 seasons in the well-instrumented Illgraben torrent in Switzerland, to investigate the challenges related to defining the radius of curvature. Furthermore, we present the preliminary results of an analysis of appropriate *k*-values to fit the superelevation velocities to the measurement station velocities. During the debris flow season of 2022, additional data has been collected using newly installed, high-resolution LiDAR scanners along the torrent in addition to the continued collection of high-resolution drone-based images, both of which are expected to contribute to further insights.

2 Site description

The well-known Illgraben torrent in canton Valais, Switzerland, has been instrumented and monitored since the year 2000 [10, 11]. Along the channel a large number of check dams have been constructed to stabilise

* Corresponding author: amanda.aaberg@wsl.ch

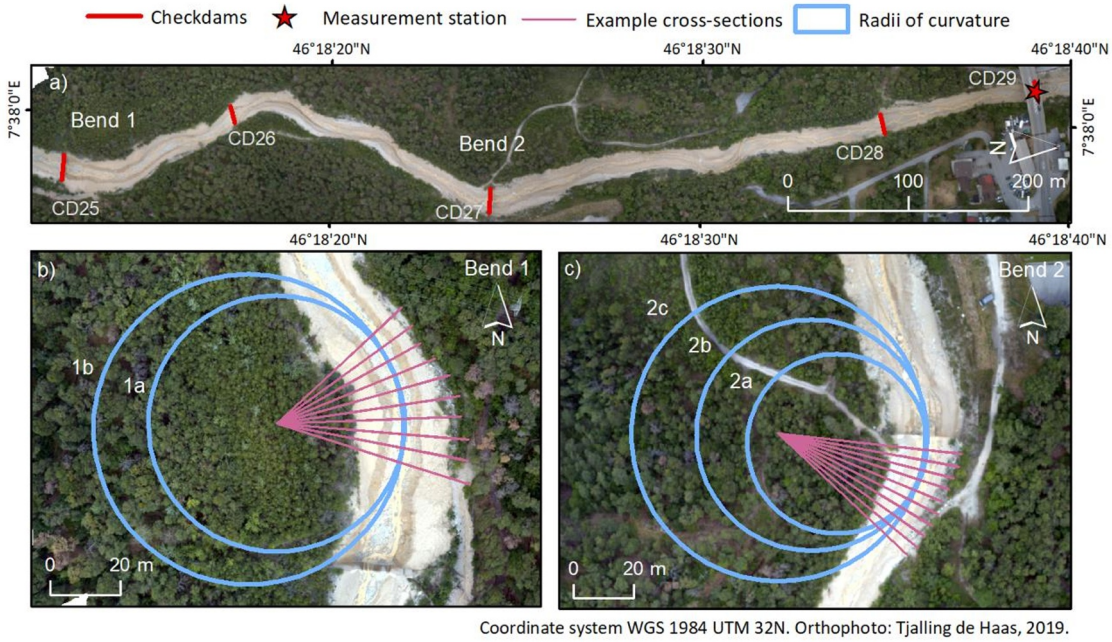

Fig 1. Overview figure of the study location: a) orthophoto from the lower section of the Illgraben torrent with locations of check dams, the measurement station at CD29 and the investigated bends (flow direction from left to right), b) bend 1 with the two tested radii of curvature and cross-sections used to collect Δh for radius 1a, c) bend 2 with the three tested radii of curvature and cross-sections used to collect Δh for radius 2c.

this active torrent. The measurement station where data on bulk flow properties are collected is located at the distal end of the fan at check dam (CD) 29, shortly before the channel's confluence with the river Rhône (Fig. 1). The superelevation analysis presented here focuses on two bends; one located in immediate proximity to CD27 approximately 480 m from CD29, and the other 340 m further upstream, shortly downstream of CD25 (Fig. 1).

3 Methods

3.1 Superelevation extraction

Extraction of superelevation values was conducted in ESRI ArcMap 10.8.1 using orthophotos and DEM's with a resolution of 5 to 10 cm from the 2019-2021 debris flow seasons [12, 13]. This topographic data has a typical error <10 cm in x, y and z directions. For each season a channel centreline was defined along a Euclidian midpoint between the channel banks using the orthophotos. Two bends were then selected for this initial analysis based on their relative proximity to the measurement station and their lack of overly steep banks to help facilitate mudline identification. A range of radii were manually fitted to these bends, such that the smallest and largest plausible radii of curvature were estimated (Fig. 1). Each bend radius was then fitted with 10 cross-sections evenly spaced along its arc length. For bend 2, which is interrupted by a check dam, all cross-sections were placed upstream of the check dam and, hence, do not cover the full arc length. The mudline elevations were then manually collected in the inner and outer bend for each cross-section using the orthophotos and corresponding DEM's. This resulted in data for superelevation, Δh, for a total of 10 debris flow events, though the number of cross-sections with reliable data range from four to 10 for the different events.

3.2 Reference velocities

The superelevation velocity has been compared to velocity estimates obtained using geophone detection of the front arrival at various check dams. Results presented here are based on the measurements obtained from travel times between CD27 and CD28, which is the nearest available segment to the investigated bends. The instrumentation for velocity estimates was re-installed in 2019 and is sometimes affected by problems related to interpretation of the geophone signals. Consequently. three events have been removed from the analysis.

3.3 Superelevation velocities and *k*

Superelevation velocities for each event were calculated using eq. 1 and $k = 1$. These velocities have then been used to examine the influence of differing radius of curvature. Additionally, for each event and each bend, k-factors were back-calculated for all available cross-sections, and a mean k and its standard deviation were thus derived for each bend and event, averaging the values obtained using different bend radii. This standard deviation represents some of the uncertainty in the Δh and B estimates, but does not incorporate the uncertainty related to the geophone velocities. The back-calculated k-factors were then compared to various flow bulk properties including Froude numbers, which were calculated using the same front velocity and a corresponding frontal flow depth obtained at CD29 using a radar sensor.

4 Results and discussion

In this study, the variability in the estimated superelevation velocities resulting from using different radii of curvature was limited, with the maximum difference between the medians for the same bend being approximately 1 m/s (Fig. 2). Meanwhile, the velocities calculated for individual cross-sections can vary considerably for the same bend and event. Local topographical features have a large influence on individual superelevation measurements, indicating that careful consideration of local topography is necessary when choosing locations for cross-sections and that ideally, many cross-sections should be used to achieve a reasonable mean value for Δh in a bend.

The back-calculated k-factors ranged between 0.83 and 7.00 (Table 1), with the exception of one extreme outlier that was likely the results of a faulty front arrival measurement. Though k should be equal to or exceed 1 [8], the standard deviation indicates that a value of 1 is within the range of the uncertainties for the one event with $k < 1$. The front velocities measured between CD27 and 28 were used as reference velocities due to the proximity to the investigated bends. Because they are often slightly lower than those measured immediately before the measurement station, they also produce fewer k-factors < 1, which are therefore more in line with those proposed in the literature.

Event 2, which displays the largest k-factor, shows a significant discrepancy between the velocities obtained between CD27-28 and CD28-29 and based on video observations, the CD28-29 velocity is overestimated. The event did not have a clear front, but 1.7 m/s was deemed to be a reasonable velocity for the early stages of the flow, whilst surges producing the maximum mudline elevation during following stages more likely had velocities of approximately 4 m/s at CD29. With the extracted superelevation such a velocity would have resulted in $k = 1.26 \pm 0.61$ for bend 1 and 0.89 ± 0.71 for bend 2, significantly lower than those based on the geophone velocities (Table 1).

Surprisingly, no clear relationships were identified between the back-calculated k-factors and other variables related to flow depth or bulk density, but k does appear to be correlated with the Froude number (Fig. 3). This nonlinear relationship supports the results of [5, 13], which were based on experimental work and field observations at Illgraben.

Superelevation velocities derived from the individual cross-sections at bend 2 show an accelerating trend toward the check dam. We attribute this to the

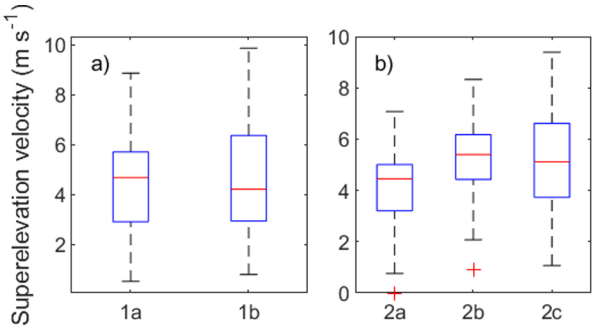

Fig. 2. Boxplots illustrating the differences in median values for superelevation velocities calculated using a constant k-factor of 1 and variable radii of curvature for: a) bend 1 with two radii of curvature and b) bend 2 with three radii of curvature. The number of data points for each radius is: 1a – 79 points, 1b – 73 points, 2a – 68 points, 2b – 58 points, 2c – 46 points.

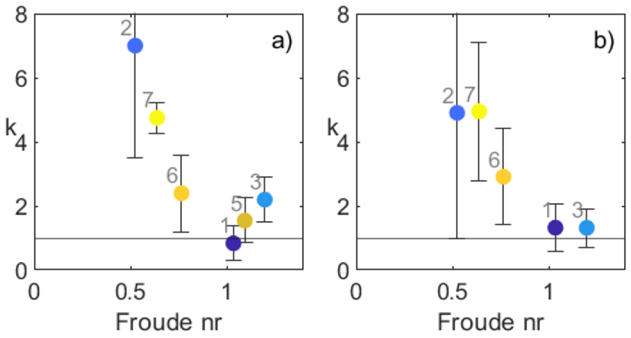

Fig. 3. Back-calculated k-factors for each event and bend using the front velocity estimate from CD27 to CD28 plotted against corresponding Froude number for a) bend 1 and b) bend 2. Error bars show standard deviations and k = 1 is marked with a solid line. Numbers reference events as listed in table 1.

Table 1. Velocities based on travel times between geophones, Froude numbers, back-calculated k-factors and superelevation velocities calculated using eq. 1 and $k = 1$ for the seven debris flow events for which front velocities between CD27 and CD28 were available. Numbered subscripts for k and superelevation velocities denote bend location.

		Geophone velocities					Superelevation velocities	
	Date	$v_{CD28-29}$ (m/s)	$v_{CD27-28}$ (m/s)	Fr nr	$k_1 \pm$ st. dev	$k_2 \pm$ st. dev	v_1	v_2
1	2019-06-21	6.62	5.32	1.04	*0.83*** ± 0.53	1.32 ± 0.72	4.59	5.89
2	2019-07-26	8.69	1.7	0.52	7.00 ± 3.49	4.90 ± 3.91	4.34	3.45
3	2019-08-11	6.95	5.16	1.20	2.19 ± 0.71	1.32 ± 0.60	7.55	5.77
4	2020-06-29	1.23	0.6	0.18	*	-	2.58	-
5	2021-06-24	8.18	5.41	1.09	1.54 ± 0.70	-	6.44	-
6	2021-07-16	2.78	3.08	0.77	2.39 ± 1.20	2.91 ± 1.50	4.62	5.04
7	2021-08-07	2.32	2.41	0.64	4.75 ± 0.49	4.95 ± 2.16	5.24	5.23

* Unreliable velocity data for CD27-28 producing unreasonably large k-factor.
** [8] indicates that k values should be >= 1, the value here likely results from uncertainties in the estimation procedure.
- Superelevation data missing.

presence of a hydraulic draw-down effect as the flow approaches the check dam, and this will be investigated further using LiDAR data collected during the 2022 debris flow season.

The distance between the locations of the investigated bends and the channel segment along which the front velocity is estimated may introduce some errors. Velocities obtained between CD27 and 28 are often slightly lower than those between CD28 and 29 (Table 1), and one of the bends is located at an additional distance upstream. Additionally, the maximum velocity and flow depth may not necessarily occur at the flow front for Illgraben debris flows, where events often lack a well-defined bouldery front. In ongoing work, the LiDAR sensors will enable a more accurate determination of the local debris flow velocity, specifically at bend 2.

Additionally, disturbances to the flow due to local irregularities may produce crossing wave fronts leaving multiple mud traces on the channel banks [14]. When affected by such phenomena, the post-event mudlines do not represent the maximum cross-channel inclination of the flow surface. The influence of such effects along with splashing caused by turbulent flow or roll-waves will likewise be examined further.

5 Conclusions and outlook

The accuracy of the forced vortex equation for estimating debris flow velocity was investigated by comparing existing velocity estimates from the measurement station with those calculated using the forced vortex equation, based on an analysis of mud line elevations extracted from bends using high-resolution UAV imagery. The definition of the bend radii has been highlighted as a source of uncertainty [9] and, though relevant, the preliminary results presented here indicate that the choice of cross-section locations and the value of k are far greater sources of uncertainty in the superelevation approach to velocity estimation. Similar to the work of [5, 8], k-factors back-calculated here approached 1 for supercritical flow and became increasingly large for subcritical flow and decreasing Froude numbers.

Despite the rare level of monitoring and data available from the Illgraben torrent, the use of the superelevation method to assess debris flow velocities is challenging. During the debris flow season of 2022, data will continue to be collected using improved measurement methods at CD29, along with UAV-based topographical data and orthophotos. Additionally, a number of newly installed LiDAR sensors will facilitate observations of front flow velocities and continuous observations of surface velocity vectors, flow depths, and flow surface geometry [15, 16]. Detailed pre- and post-event topography will be available, along with the timing of maximum flow depth and surface inclination as well as the presence and timing of surges and cross-wave maxima. This data will thus provide a new window into the physical meaning of the k-factor and hopefully enable improvements to the accuracy of velocity estimates obtained through the superelevation method.

References

1. L. Bugnion, B.W. McArdell, P. Bartelt and C. Wendeler, Landslides **9**, 2, pp.179-187 (2012)
2. J.E. Costa, *Physical geomorphology of debris flows*, in Developments and applications of geomorphology, pp. 268-317, Springer, Berlin, Heidelberg (1984)
3. S.P. Pudasaini, M. Jaboyedoff, Landslides **17**, 6, pp.1377-1392 (2020)
4. O. Hungr, G.C. Morgan, R. Kellerhals, Can. Geotech. J. **21**, 4, pp. 663-677 (1984)
5. C. Scheidl, B. McArdell, G. Nagl, D.Rickenmann, *Debris flow behavior in super-and subcritical conditions,* in 7th International Conference on Debris-Flow Hazards Mitigation (2019)
6. D.F. VanDine, Res. Br., BC Min. For., Victoria, BC, Work. Pap. **8** (1996)
7. M.H. Bulmer, O.S. Barnouin-Jha, M.N. Peitersen, M. Bourke, *J. Geophys. Res. Planets* **107**, E5, pp.9-1. (2002)
8. C. Scheidl, B.W. McArdell, D. Rickenmann, Can. Geotech. J. **52**, 3, pp. 305-317. (2015)
9. A.B. Prochaska, P.M. Santi, J.D. Higgins, S.H. Cannon, Landslides **5**, 4, pp. 431-444 (2008)
10. M. Hürlimann, D. Rickenmann, C. Graf. Can. Geotech. J. **40**, 1, pp. 161-175 (2003)
11. B.W. McArdell, Int. J. Eros. Control Eng. **9**, 4, pp.194-198 (2016)
12. T. de Haas, W. Nijland, B.W. McArdell, M.W. Kalthof, Front. Remote Sens. **2**, p.5 (2021)
13. T. de Haas, B.W. McArdell, W. Nijland, A.S. Åberg, J. Hirschberg, P. Huguenin, Geophys. Res. Lett. **49** (2022)
14. T.C. Pierson, *Geol. Soc. Am. Bull.* ***96***, 8, pp.1056-1069 (1985)
15. J. Aaron, R. Spielmann, B. McArdell, C. Graf DFHM8, submitted (this proceedings volume)
16. R. Spielman, J. Aaron, B. McArdell, DFHM8, submitted (this proceedings volume)